THE REMBRANDT TROUGH: EVIDENCE OF LITHOSPHERIC FOLDING ON MERCURY? Thomas R. Watters[1], Sean C. Solomon[2], Jürgen Oberst[3], Frank Preusker[3], Steven A. Hauck, II[4], and Maria T. Zuber[5]. [1]Center for Earth and Planetary Studies, National Air and Space Museum, Smithsonian Institution, Washington, DC 20560, USA (watterst@si.edu); [2]Lamont-Doherty Earth Observatory, Columbia University, Palisades, NY 10964, USA; [7]German Aerospace Center, Institute of Planetary Research, D-12489 Berlin, Germany; [4]Department of Earth, Environmental, and Planetary Sciences, Case Western Reserve University, Cleveland, OH 44106, USA; [5]Department of Earth, Atmospheric and Planetary Sciences, MIT, Cambridge, MA 02139, USA.

Introduction: The Rembrandt impact basin was discovered during the second Mercury flyby by the MErcury Surface, Space ENvironment, GEochemistry, and Ranging (MESSENGER) spacecraft [1]. At ~715 km in diameter, it is the second-largest well-preserved impact basin known on Mercury. The age of the Rembrandt basin is comparable to that of the larger Caloris basin [1]. Like Caloris, Rembrandt is partially filled with volcanic plains. In addition to a complex array of basin-radial and basin-concentric wrinkle ridges and graben, the western rim and floor of Rembrandt are crosscut by the largest lobate scarp on Mercury [1]. MESSENGER's third flyby revealed a second large lobate scarp to the south that trends sub-parallel to the first scarp. Topographic data derived from MESSENGER orbital stereo images [2] indicate that the two scarps form the flanks of a broad valley, the eastern end of which is near Rembrandt's southwestern rim. This broad, long-wavelength feature provides insight into the large-scale deformation of Mercury's lithosphere.

Topography of the Trough and Scarps: Stereo images obtained from the Mercury Dual Imaging System (MDIS) wide-angle camera (WAC) and narrow-angle camera (NAC) have been used to generate digital terrain models (DTMs) with a lateral spacing of 250 m/pixel and a vertical accuracy of about 30 m [2]. The DTM for the area clearly shows the major topographic features associated with the Rembrandt basin, the two large lobate scarps, and the broad trough (Fig. 1). Topographic data indicate that the northern scarp has >2 km of relief where it transects the basin interior floor, and slopes on the scarp face are >30º in some areas (Fig. 2). The broad valley extends for ~1000 km (Fig. 1) and passes through the southwestern section of the basin rim, where the rim appears to be lower than elsewhere, into the basin interior. The topographic data show that the southern scarp is ~450 km long and has an orientation approximately parallel to the northern scarp. The width of the trough varies from ~270 km near the basin rim to a maximum of ~480 km; much of the trough is ~450 km wide. Slopes on the bounding scarps are generally greater than 10°, including segments within the Rembrandt basin interior, whereas slopes in the valley are generally less than 5°. The depth of the trough also varies and exceeds 3 km in some locations (Fig. 2).

Interpretation and Modeling: The topographic data suggest that the broad valley is bounded by opposite-vergence thrust faults (Figs. 1, 2). The association of the valley and lobate scarps suggests that these structures may have formed in connection with long-wavelength folding of the lithosphere. A small deflection of the lithosphere due to low-amplitude folding might have localized the opposite-vergence faults and contributed to the generally uniform, lower relative elevation of the valley. Buckling instability models have been used to account for the localization of spaced faults elsewhere [3, 4]. Localization instability models can also account for regularly spaced faults [5, 6]. If the trough is the result of lithospheric folding that occurred at a critical wavelength, its width reflects the mechanical properties of the lithosphere at the time of deformation. Interior structure models consistent with Mercury's moments of inertia indicate that the outer silicate shell of the planet is ~420 km thick and may be underlain by a layer of solid FeS atop the fluid outer core [7, 8]. The width of the trough at Rembrandt is thus similar to the thickness of the mantle plus crust. To pursue this idea, we model Mercury's lithosphere as a single elastic member (thickness h) or a multilayer (nh) that buckled at a critical wavelength of folding as a result of layer instability [4]. An elastic lithosphere of Young's modulus E is taken to rest on a mechanically weak elastic mantle with modulus E_0 and density ρ_0. The asthenosphere, defined as the inviscid portion of the outer silicate shell, is of finite thickness (h_0) and is assumed to overlie a solid FeS layer that is rigid and does not participate in the deformation. However, the validity of this last assumption is difficult to test with available data. As the ratio $E_0/(\rho_0 g h_0)$ approaches zero, where g is the gravitational acceleration, the equation for the critical wavelength reduces to the solution for an elastic plate floating on a fluid [4]. Model results show that a wavelength of ~450 to 500 km can be obtained for a range of thicknesses of the elastic lithosphere (T_e ~35-60 km) with a strength contrast E/E_0 = 1000 (equivalent to the case of a fluid mantle) and h_0 = 400 km (Fig. 3). Large critical stresses predicted by elastic buckling models can be reduced to values below the frictional strength if the lithosphere behaves as a multilayer. Arcuate lobate scarps with distinct bow-like shapes (e.g., Beagle Rupes) may involve listric faults that sole in a zone of weakness within the lithosphere [9]. A zone of weak-

ness in the lithosphere may provide a mechanical basis for a two-layer model.

Modeling of the depth of faulting of large-scale lobate scarp thrust faults and analysis of dynamic localization mechanisms suggest that the thickness of the elastic lithosphere at the time of thrust faulting was ~30–60 km [10-12]. Thus, there is agreement between the value of T_e obtained from the folding model and independently determined values. Analysis of the sensitivity of the critical wavelength to the thickness of the asthenosphere shows that this wavelength depends on the strength contrast. The wavelength of folding is not sensitive to expected values of asthenosphere thickness (h_0 > 100 km for T_e = 40 km and a weak or fluid mantle). Thus, the presence or absence of a solid layer of FeS at the core-mantle boundary should not influence long-wavelength folding of the lithosphere.

Crosscutting relations between the lobate scarps and the Rembrandt basin rim and floor [1] and the relatively low elevation of the southwestern rim indicate that at least a portion of the trough and scarp development likely postdated the formation of the basin and basin infilling. This timing suggests a post-Calorian age for the trough and scarps. Data from the Mercury Laser Altimeter (MLA) and from stereo imaging [13] have revealed other long-wavelength topographic variations on Mercury [14, 15]. One of these is a broad rise almost 1000 km across with ~1.5 km of relief in the northern smooth plains [15]. Those plains are Calorian in age [16], and the rise appears to postdate their emplacement [15] and may also postdate subsequent wrinkle ridge deformation. Thus, like the northern rise and other long-wavelength modifications of Mercury's topography, the development of the scarps and trough near the Rembrandt basin occurred after the formation of the youngest large impact basins and the emplacement of the Calorian smooth plains.

References: [1] Watters T.R. et al. (2009) *Science*, *324*, 618-621. [2] Preusker F. et al. (2012) *EPSC Abstracts*, *7*, 2012-528. [3] Zuber M.T. and Aist L.L (1990) *JGR*, *95*, 14,125–14,230. [4] Watters T.R. (1991) *JGR*, *96*, 15,599-15,616. [5] Montési L.G.J. and Zuber M.T. (2003) *JGR*, *108*, doi:10.1029/2002JB001923. [6] Montési L.G.J. and Zuber M.T. (2003) *JGR*, *108*, doi:10.1029/2002JB001924. [7] Smith D.E. (2012) *Science*, *336*, 212-216. [8] Hauck S.A., II, et al. (2012) *JGR*, submitted. [9] Rothery, D.A. and M. Massironi (2010) *Icarus*, *209*, 256-261. [10] Watters T.R. et al. (2002) *Geophys. Res. Lett.*, *29*, doi:10.1029/2001GL014308. [11] Nimmo F. and Watters, T.R. (2004*) Geophys. Res. Lett.*, *31*, doi:10.1029/2003GL019171. [12] Zuber M.T. et al. (2010) *Icarus*, *209*, 247-255. [13] Oberst J. et al. (2010) *Icarus*, *209*, 230-238. [14] Solomon S.C. et al. (2012) *Lunar Planet. Sci*., *43*, 1578. [15] Zuber et al. (2012) *Science*, *336*, 217-220. [16] Head J.W. et al. (2011) *Science*, *333*, 1853-1856.

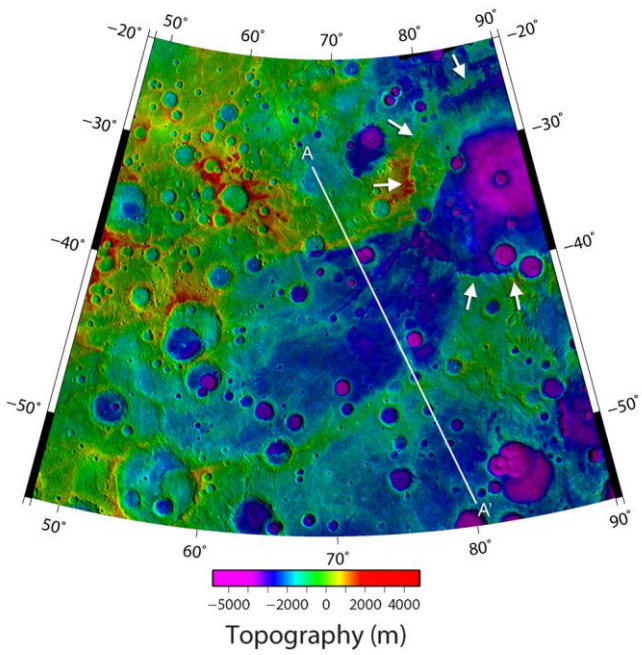

Figure 1. DTM derived from MDIS orbital stereo images. The white line shows the location of the profile given in Fig. 2. White arrows show the location of the Rembrandt basin rim.

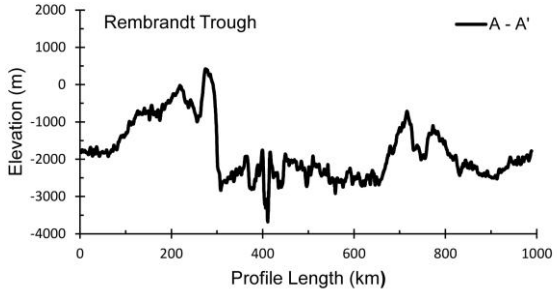

Figure 2. Topographic profile across the Rembrandt trough. The width of the trough at this location is ~440 km, and the depth exceeds 3 km. Profile location is shown in Fig. 1. Elevations are relative to a sphere of radius 2440 km.

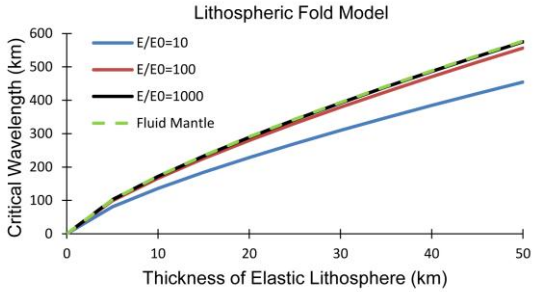

Figure 3. Critical wavelength of folding as a function the thickness of the elastic lithosphere. The lithosphere and mantle density are taken to be 3000 and 3300 kg m^{-3}, respectively.